PHOTON DOPPLER VELOCIMETRY NOISE SUPPRESSION ALGORITHM BASED ON DIFFERENTIAL COMPENSATION

Jinbao FENG[1,2*], Yubin GAO[3], Gao WANG[4], Jinhui WU[5]

A dual-probe structure is designed, and a differential compensation algorithm is proposed. It can effectively suppress the noise of Photon Doppler Velocimetry(PDV). Through the differential compensation algorithm, the test data is iteratively related to the signal, and the correction of the test speed inversion is realized. The experimental targets with different speeds are tested. From the position change curve, it is known that the position accuracy is higher after the differential compensation algorithm is used, and the speed test fluctuation is increased from 10.25% to 2.43% compared with the non-compensation method. Using this algorithm can effectively improve the signal noise suppression capability.

Keywords: Photon Doppler Velocimetry (PDV); Differential Compensation; Velocity Test; Noise Suppression

1. Introduction

Velocity detection of high-speed small targets has been a wide concern in the military, scientific research and industrial applications, and with the continuous development of optical information processing technology, Photonic Doppler Velocimetry (PDV, Photonic Doppler Velocimetry) [1-4] due to its characteristics of non-contact, high sensitivity and good stability. It becomes one of the research hotspots in the direction of transient speed measurement.

The Lawrence Livermore National Laboratory in the United States [5-8] used PDV technology to study ultra-high-speed fragments and projectiles. It was proposed to use chirped pulses instead of continuous lasers to obtain higher temporal resolution. The industrial-grade vibration velocity test system launched by the German Polytec Group had a maximum vibration velocity measurement value of 2000mm/s and an effective distance of 3m [9]. Frogget B. C. et al. [10] modified the lens of PDV and adopted a fish-eye design, which greatly improved

[1] Lecturer, School of Information and Communication Engineering, North University of China, e-mail: 42395446@qq.com
[2] Lecturer, Maths & Information Technology School, Yuncheng University, China, e-mail: 42395446@qq.com
[3] Prof., School of Science, North University of China, e-mail: ybgao@nuc.edu.cn
[4] Prof., School of Information and Communication Engineering, North University of China, e-mail: wanggao@nuc.edu.cn
[5] Prof., School of Instrument and Electronics, North University of China, e-mail: wujinhui@nuc.edu.cn

the photon collection efficiency. Malone R. M. et al. [11, 12] proposed a structural design scheme for slopping the fiber end face to improve the light propagation efficiency. Song HW et al. [13] obtained the low-speed fringe signal of PDV by applying the filtering method of continuous wavelet transform to Fourier transform, thereby improving the signal-to-noise ratio of the system. Ma Heli et al. [14] applied PDV to the inner diameter measurement of small-diameter long-body structures, and the measurement error of 200mm was only 14μm. Peng Yingcheng et al. [15] used PDV to construct a vibration-sensing structure with a depth of field ±2 cm. Neemat S. et al. [16] designed a composite optical fiber heterodyne interference structure, the measurement accuracy of which can reach 6 nm in the range of 100μm.

PDV technology is used in high-speed target detection due to its strong anti-interference ability, large speed measurement range and high stability. However, when the space optical signal enters the optical fiber, it is interfered with by the incident angle, surface reflectivity, shock wave oscillation, etc., which must contain a large number of noise signals. The purpose of this paper is to improve the noise suppression capability of the PDV system, so that it can better complete the inversion of moving target velocity. Firstly, the structure of the optical fiber probe is optimized systematically, and a dual-channel probe structure with optical fiber axis symmetry is designed. Then, the correlation operation is performed on the data collected by different probes, thereby superimposing the effective signals, and completing the noise suppression through differential compensation.

2. System design

The system adopts an all-fiber heterodyne sensing structure in Fig. 1.

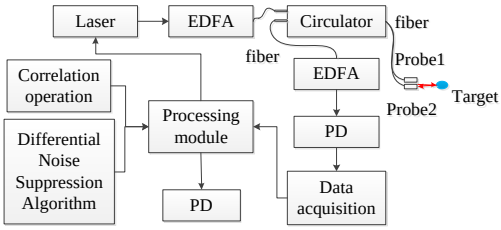

Fig. 1. Structure diagram of the improved PDV system

The light source is a 20.0 kHz narrow linewidth laser with a central wavelength of 1550.0nm and an output power of 14.0mW. An Erbium Doped Fiber Amplifier (EDFA [17]) is used to amplify the laser signal, and then it enters the area to be measured through an optical circulator. When the target enters the test area, due to the high speed of the target, an obvious Doppler phenomenon [18] would occur. The resulting frequency shift can be picked up by the sensor. Finally, it is transmitted to the processing system by the data acquisition module.

The PDV noise suppression algorithm based on differential compensation is preset in the processing system, and the effective signal extraction is realized by the correlation operation and differential superposition of multiple sets of echo signals.

3. Algorithm design

3.1 Principle of the system

The PDV system is implemented using the all-fiber Michelson interference principle. According to the Doppler principle, the average output intensity of the laser is:

$$I(t) = I_0^2(t) + I_d^2(t) + 2\sqrt{I_0(t) + I_d(t)} \cdot \cos\left(2\pi \int_0^t \frac{2v(t)}{\lambda_0} dt + \varphi_0\right) \tag{1}$$

Among them, t is the time, $I_0(t)$ is the intensity of the reference laser, $I_d(t)$ is the intensity of the signal light, φ_0 is the initial phase difference, $v(t)$ is the target speed; λ_0 is the laser wavelength. The function of the test optical signal about the target displacement and velocity is:

$$f(t) = \frac{2v(t)}{\lambda_0} \tag{2}$$

The signal must meet the zero mean condition before it can be used for time-frequency analysis. Therefore, let the prototype wave be $\Psi(t)$, then

$$\psi_{(b,a)}(t) = \frac{1}{a}\psi\left(\frac{t-b}{a}\right), b \in R, a > 0 \tag{3}$$

Among them, a is the scale factor and b is the time factor. When a>1, the window function frequency is compressed, and conversely, when a<1, the window function frequency is stretched. The continuous wavelet transform of the signal s(t) is:

$$W(b,a) = \int_{-\infty}^{+\infty} s(t)\psi_{(b,a)}(t)dt \tag{4}$$

The time velocity function of the signal $s(t)$ can be obtained by inversion.

3.2 Differential compensation design

Since there is a deflection angle between the target to be measured and the probe, it is necessary to analyze the return loss caused by the deflection angle. The return loss of the system can be expressed as

$$R_t = -10\log\frac{P_r}{P_i} \tag{5}$$

Among them, R_t is the power reflection coefficient of the fiber end face, and P_r and P_i are the reflected optical power and the incident optical power. When the

return loss is larger, the reflected light power is smaller under the same incident light power. For single-mode fiber, when the angle between the two detectors is α, the reflection coefficient can be expressed as

$$R = R_0 \exp\left[-\left(\frac{\pi n \omega 2\alpha}{\lambda}\right)^2\right] \tag{6}$$

Among them, α is the angle between the two detectors, R_0 is the Fresnel reflection coefficient, λ is the wavelength, ω is the phase parameter, and n is the refractive index of the fiber.

3.3 Probe differential structure

The probe structure of the system is optimized. A sensor with an angular deflection of α is simultaneously placed on the original probe position, thus forming a dual-probe structure. Its structure is shown in Figure 2. The optical signal collected by probe 1 is denoted as F(t). The test signal on probe 2 has a correlation with that on probe 1, and the influence factor of the correlation function is α, so the optical signal on probe 2 is recorded as F(t)*$f(\alpha)$.

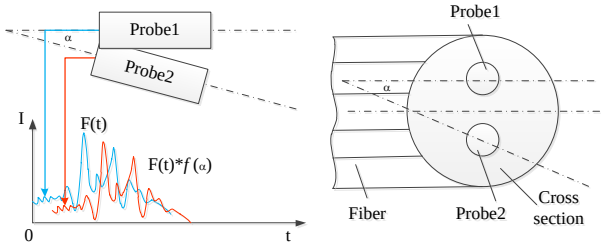

Fig. 2. Structure optimization of the front-end face

It can be seen from Figure 2 that the two groups of signals are iterated to generate the correlation function:

$$R_{W_1W_2}(\tau) = \lim_{T\to\infty} \frac{1}{T} \int_0^T W_1(t) W_2(t)\, dt \tag{7}$$

Among them, W_1 and W_2 are the echo signals collected by probe 1 and probe 2, respectively. Then, the correlation function is used to superimpose the data that conforms to the correlation, and the data that does not conform to the correlation is subtracted, to suppress the noise. Using the correlation function, the "positive correlation calculation" can be performed on the signals collected in the two groups of sensors. The calculated correlation degree can represent the correlation between the two sets of data, and then the positions with signal characteristics can be extracted according to the magnitude of the correlation degree, to subtract other irrelevant signals containing noise. The correlation operation is often used in mathematics. It is calculated by iterating over data with similar frequencies and

amplitudes between two sets of signals, thereby reducing the impact of uncorrelated noise on the test data.

4. Simulation analysis

4.1 Signal light energy distribution

The received light energy can be analyzed under the condition of a fixed angle α by ZEMAX. The position of probe 1 is set as the position of the optical axis, and probe 2 is at the position with a declination angle of α from the optical axis. The optical system parameter settings are shown in Tab. 1.

Table 1

Parameter setting table of receiving optical structure

Type	Radius	Thickness	Glass	Semi-Diameter
OBJ	Infinity	Infinity	-	Infinity
STO	11.205148	1.000000	BK7	2.025545
2	-65.215487	96.548125	-	1.958715
3	274.254865	4.000000	-	8.885487
4	48.362587	10.000000	BK7	9.065284
IMA	Infinity	-	-	9.015487

The simulation results are shown in Fig. 3.

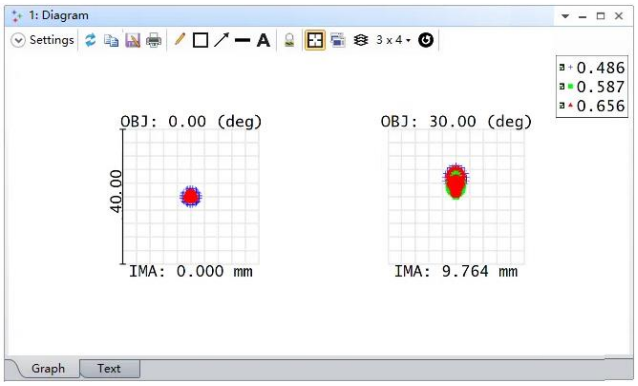

Fig. 3. Column diagram of light spots under the condition of declination

It can be clearly seen from the energy distribution in Fig. 3. When probe 1 has no deflection angle, the speckle pattern distribution of probe 1 is very uniform, and the energy is mainly concentrated in the center of the fiber core diameter. Compared with probe 2, which has a declination angle (the declination

value is set to 2° in the simulation, which is consistent with the arrangement position of the actual probe), the light spot is obviously shifted, and the energy distribution is no longer uniform. It can be seen that when the deflection angle α is introduced, the two sets of detection data will be different, and the correlation factor between the two sets of data is the function of α.

4.2 Probe structure parameters

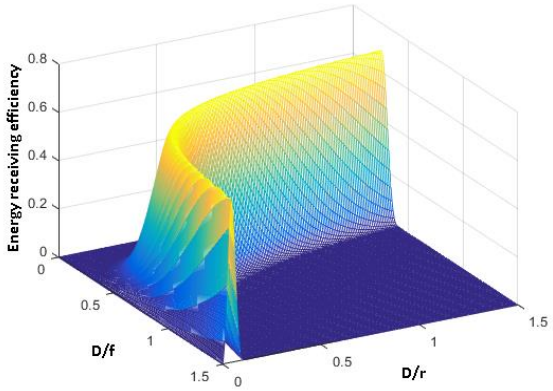

Fig. 4. Relationship between energy receiving efficiency and probe parameters

In addition to the angle between the probe and the target to be measured, which will affect the system test results, the structure of its surface will also affect the probe energy. The microlens diameter *D*, lens focal length *f* and core diameter *r* of the fiber end face are the main parameters that affect its energy. And the three parameters do not affect the light wave energy independently. Among them, the ratio *D*/*f* of the diameter of the microlens to the focal length determines the energy concentration, and the ratio *D*/*r* of the diameter of the microlens to the diameter of the core determines the receiving field of view. Assuming that the variation range of *D*/*f* is (0, 1.5) and the size variation range of *D*/*r* is (0, 1.5), the energy receiving efficiency is shown in Fig. 4.

The energy-receiving efficiency varies with *D*/*f* and *D*/*r*. That is, when the position and angle of the structure to be tested are different, the energy receiving efficiency will be affected. When *D*/*r* is a fixed value, *D*/*f* will generate a peak. When *D*/*r* is between (0, 0.5), the peak position of *D*/*f* is concentrated in the interval of (1, 1.5), and the peak width is large, and the mean value is around 0.44. When *D*/*r* is between (0.5, 1.5), the peak position of *D*/*f* is concentrated in the interval of (0, 0.5), and the peak width is small, and the mean value is around 0.23. When *D*/*f* is a fixed value, *D*/*r* also produces a peak. When *D*/*f* is between (0, 0.5), the peak position of *D*/*r* is concentrated in the interval of (1, 1.5), and the peak width is large, and the mean value is around 0.83. When *D*/*f* is between (0.5, 1.5), the peak position of *D*/*r* is concentrated in the interval of (0, 0.5), and the

peak width is small, and the mean value is around 0.15. It can be seen that the change trends of the two parameters are similar.

5. Experiment

5.1 Experimental conditions

In the experiment, the rodless cylinder is used to obtain the adjustable speed of the target, and the PDV is used to measure the shock speed process [19]. On the rodless cylinder, the piston is connected with the slider to realize reciprocating motion, thereby forming a target to be measured with an adjustable speed of 12-14m/s. The cylinder frame and detection device are shown in Fig. 5.

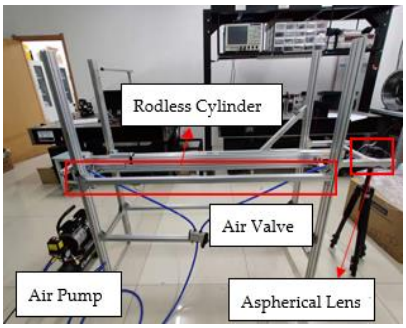

Fig. 5. Experimental system

5.2 Data acquisition preprocessing

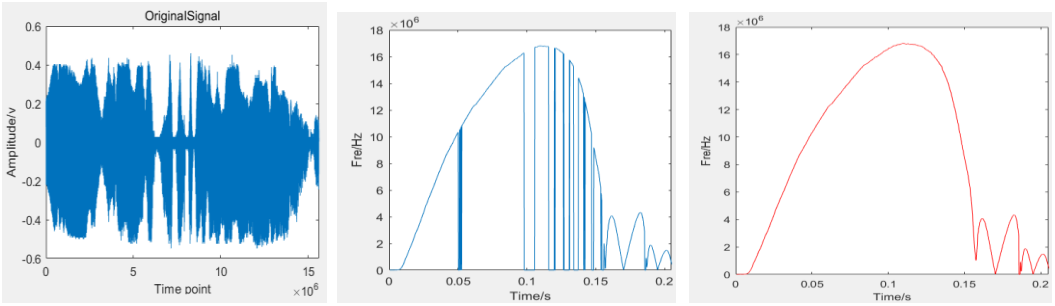

(a) Raw data signal (b) Without preprocessing (c) With preprocessing

Fig. 6. Comparison of response curves before and after preprocessing optimization

In the experiment, the data acquisition rate is 200MHz, and the spectrum of the acquired data is analyzed by Fourier transform. The original data is shown in Figure 6(a), but since the original data contains a lot of noise, it is necessary to suppress and smooth the noise. If the preprocessing before data processing is not adopted, the frequency spectrum line is directly inverted, as shown in Fig. 6(b). However, using preprocessing to filter the data signal first, the frequency spectrum line is inverted, as shown in Fig. 6(c).

It can be seen from Fig. 6(a) that in the spectrum curve before preprocessing, the energy values of many frequency positions are disturbed and cannot be obtained by calculation. When the signal is patched with preprocessing, the overall curve became smooth and continuous, as Fig. 6(b). The preprocessing method is the modulo maximum extraction frequency correction algorithm. The algorithm first classifies the mutation interval of the curvature position in the curve, and conducts pattern analysis on the corresponding interval. It supplies the corresponding interpolation amount in the corresponding interval, and finally makes the curves connect smoothly. The filter window length is 65536, and the operating frequency of the FFT transform at the last FFT frequency is 14MHz. Calculating with the next FFT energy weighting produced at that frequency, an interpolation for that velocity curve can be obtained.

5.3 Comparison of differential compensation optimization

In the experiment, the single-probe test data (SPT, Single Probe Test) and the dual-probe differential compensation test data (DCT, Differential Compensation Test) are used to compare, and the velocity inversion values of the two methods are tested under different velocities of moving targets. Error analysis is carried out for the standard speed, and the results are shown in Fig. 7.

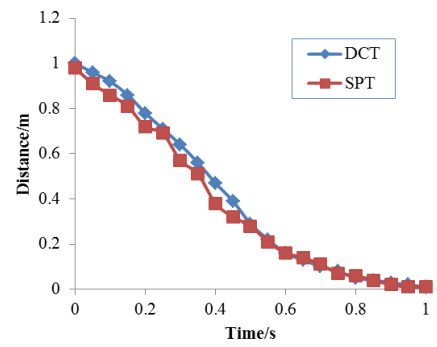

(a) Position offset

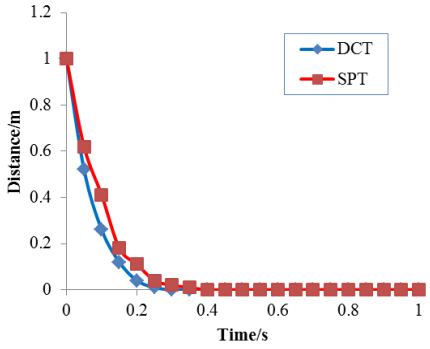

(b) Position offset

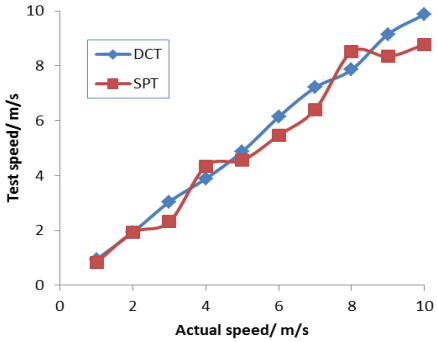

(c) Absolute speed error

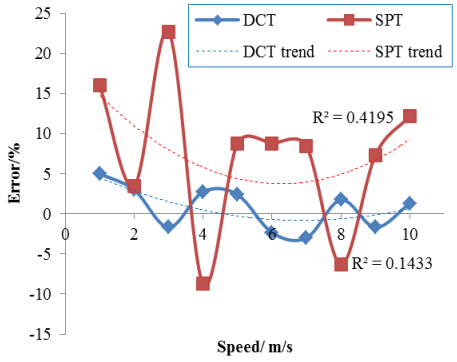

(d) Relative speed deviation

Fig. 7. Comparison before and after using differential compensation at different speeds

As shown in Fig. 7(a) and Fig. 7(b), when the test speed is 1m/s and 5m/s, respectively, the position inversion information is obtained by the DCT method and the SPT method. The two methods get a consistent trend of position change, but the curves are smooth and coherent. DCT is significantly better than SPT. It can be seen that the inversion effect of the target position after differential compensation is better, which can better suppress the noise in the test process. As shown in Fig. 7(c), in the process of increasing velocity, the inversion velocity using the DCT method has a better match with the actual velocity, while the test data using the SPT method has many sudden changes in the test data. This is due to the instability of the inversion data caused by the noise interference of the corresponding position signal. As shown in Fig. 7(d), the speed relative error of DCT has a small fluctuation range, and its average fluctuation is 2.43%, while the average fluctuation of SPT is 10.25%. Through the comparison of the fluctuation trend of the two methods, the R^2 of DCT is 0.1433, the R^2 of SPT is 0.4195, and the DCT is relatively flat.

6. Conclusions

In this paper, a differential compensation algorithm is studied based on the design of the dual-probe structure. The system uses the modulo maximum extraction frequency correction algorithm to initially optimize the original data, and then uses the differential compensation algorithm to perform correlation iteration on the effective signal, thereby suppressing noise interference. Through simulation analysis, the spot energy distribution and energy receiving efficiency curve under different declination angle conditions are obtained. The data optimization experiment and the velocity inversion comparison experiment are completed respectively. The experimental results are shown that the optimized test curve has complete continuity. The position test curve of the DCT method is smoother than that of the traditional SPT method. The abnormal fluctuations are significantly reduced in the velocity inversion curve. The algorithm has a good effect in suppressing noise interference in the process of photon Doppler velocity measurement. It can be applied to high-speed target transient speed measurement and other fields.

Acknowledgements

This research is funded by Shanxi Scholarship Council of China (Grant No. 2021-116).

R E F E R E N C E S

[1]. *E. Klejmova, J. Pomenkova*, “Identification of a Time-Varying Curve in spectrogram”, RADIOENGINEERING, **vol. 26**, no. 1, Jan. 2017, pp. 291-298.

[2]. *Zhao. Q, Qiu. W, Zhang BX, et al.*, "Quickest Spectrum Sensing Approaches for Wideband Cognitive Radio Based On STFT and CS", KSII TRANSACTIONS ON INTERNET AND INFORMATION SYSTEMS, **vol. 13**, no. 3, Mar. 2019, pp. 1199-1212.

[3]. *D. Leandro, Zhu. MS, M. Lopez-Amo, et al.*, "Quasi-Distributed Vibration Sensing Based on Weak Reflectors and STFT Demodulation", JOURNAL OF LIGHTWAVE TECHNOLOGY, **vol. 38**, no. 24, Dec. 2020, pp. 6954-6960.

[4]. *Tao. HF, Wang. P, Chen. YY, et al.*, "An unsupervised fault diagnosis method for rolling bearing using STFT and generative neural networks", JOURNAL OF THE FRANKLIN INSTITUTE-ENGINEERING AND APPLIED MATHEMATICS, **vol. 357**, no. 11, Nov. 2020, pp. 7286-7307.

[5]. *H. D. D.*, "Extreme measurements with photonic doppler velocimetry (PDV)", The Review of Scientific Instruments, **vol. 91**, no. 5, May. 2020, pp. 051501- 051510.

[6]. *G. MJ., M. LLB., H. DD., et al.*, "Time-stretched photonic Doppler velocimetry", Optics Express, **vol. 27**, no. 18, Jun. 2019, pp. 3511-3524.

[7]. *Mallick D D, Zhao M, Bosworth B T, et al.*, "A simple dualbeam time-multiplexed photon Doppler velocimeter for pressure-shear plate impact experiments", Experimental Mechanics, **vol. 59**, no. 1, Jun. 2019, pp. 1120-1128.

[8]. *Mallick D D, Zhao M, Parker J, et al.*, "Laser-driven flyers and nanosecond- resolved velocimetry for spall studies in thin metal foils", Experimental Mechanics, **vol. 59**, no. 5, May. 2019, pp. 127-135.

[9]. *Mou Xinrui, Zhang Jian, An Fei, et al.*, "Design of optical fiber array coupling system for multi-channel photonic doppler velocimetry", Optical Technique, **vol. 46**, no. 4, Apr. 2020, pp. 443-447.

[10]. *Frogget BC, Cata BM, Cox BC, et al.*, "SPIE procedures interferometry xvi: applications-a fisheye lens as a photonic Doppler velocimetry probe". Procedures of SPIE the International Society for Optical Engineering, **vol. 8494**, no. 1, Apr. 2012, pp. 84940D.

[11]. *Malone RM, Briggs ME, Cox BC, et al.*, "Design, assembly and testing of a photon Doppler velocimetry probe", Procedures of SPIE-The International Society for Optical Engineering, Optical Technique, **vol. 8131**, no. 3, Mar. 2011, pp. 813109.

[12]. *Malone RM, Cata BM, Daykin EP, et al.*, "Photonic Doppler Velocimetry Probe Designed With Stereo Imaging", Procedures of SPIE-The International Society for Optical Engineering, **vol. 9195**, no. 3, Mar. 2014, pp. 919503.

[13]. *Song. HW, Wu. XQ, Huang. CG.*, "Measurement of fast-changing low velocities by photonic Doppler velocimetry", REVIEW OF SCIENTIFIC INSTRUMENTS, **vol. 83**, no. 7, Jul. 2012, pp. 073301.

[14]. *Ma Heli, Tao Tianjiong, Liu Shenggang, et al*.,"A measuring system for inner diameter of small-caliber and long gun bore based on frequency domain interferometry", Acta Armamentarii, **vol. 40**, no. 5, May. 2019, pp. 1077-1082.

[15]. *Peng Yingcheng, Guo Xian, Chen Rong, et al*., "Design of vibration displacement sensor with inertial sliding block based on PDV technology", Instrument Technique and Sensor, **vol. 1**, no. 9, Spet. 2019, pp. 5-9.

[16]. *Neemat, S, Krasnov, O, Yarovoy, A.*, "An Interference Mitigation Technique for FMCW Radar Using Beat-Frequencies Interpolation in the STFT Domain", IEEE TRANSACTIONS ON MICROWAVE THEORY AND TECHNIQUES, **vol. 18**, no. 8, Aug. 2018, pp. 1344-1349.

[17]. *J. Huang, B. Chen, B. Yao.*, "ECG Arrhythmia Classification Using STFT-Based Spectrogram and Convolutional Neural Network", SPECIAL SECTION ON DATA-ENABLED INTELLIGENCE FOR DIGITAL HEALTH, **vol. 7**, no. 1, Jan. 2019, pp. 92871- 92880.

[18]. *Liu S, Wang D, Li T, et al*, "Analysis of photonic doppler velocimetry data based on the continuous wavelet transform", Review of Scientific Instruments, **vol. 82**, no. 2, Feb. 2011, pp. 023103.

[19]. *Feng JB, Wu JH, Si Y.*, "Reconstruction of Velocity Curve in Long Stroke and High Dynamic Range Laser Interferometry", Sensors, **vol. 21**, no. 22, Nov. 2021, pp. 7520-7537.